Agnieszka Kurc-Lisiecka, Aleksander Lisiecki

Laser Welding of High-Strength Steel S960QL

Abstract: The article discusses the results of tests concerning the effect of parameters used during the basic bead-on-plate laser welding (i.e. location of the laser beam focus, welding rate and linear welding energy) of 4.0 mm thick sheets made of high-strength steel S960QL on the quality and properties of simulated butt joints. The welding tests were performed using a YAG TruDisk 3302 Yb disk laser (TRUMPF) having a maximum output power of 3.3 kW and provided with a head focusing the laser beam spot to a diameter of 200 μm. The simulated butt welded joints were made without the filler metal, using a technique which consisted in the laser beam melting of sheets. Macroscopic and microscopic tests as well as impact strength tests, fractographic tests and microhardness measurements involved the cross-section of the simulated specimens.

Keywords: laser welding, steel S960QL, disk laser, microstructure and properties

DOI: 10.17729/ebis.2022.3/4

Introduction

Producers of steel structures and machinery, including stationary and self-propelled cranes, hoists, railway wagons, posts, poles, bridge supports, oil rigs or structural elements of cars and special vehicles, try to use materials providing a favourable weight-strength ratio. Advantages resulting from the attempted reduction of vehicle weight were discussed in detail by Li G.J. and Liu X.L. [1]. The aforesaid trend, arising from increasingly demanding customers' expectations, the necessity of decreasing production-related material consumption and energy consumption indexes, is continuously confronted with the need for the improvement of operating parameters of steel structures, their service life and reliability. Some of the structural materials improving the strength of structures without increasing the weight of the entire load-carrying structure, commonly used in industry, are advanced high strength steels (AHSS), including dual phase steels (DP), complex phase steels (CP), martensitic steels as well as steels characterised by transformation induced plasticity (TRIP) (discussed in detail by Ohjoon K. et al. [2]). High mechanical properties (e.g. yield point restricted within the range of 460 MPa to 1300 MPa; Fig. 1) of the above-named steels, resulting from their chemical compositions and applied manufacturing processes, were discussed in detail by Goss C. et al. and Urbańczyk M. et al. [3–4].

Advanced high strength steels are characterised by good weldability, yet their joining requires the precise adjustment of parameters as well as the rigorous following of technological

dr inż. Agnieszka Kurc-Lisiecka – Institute of Applied Sciences at WBS University in Poznań; Division of WBS University in Chorzów; dr hab. inż. Aleksander Lisiecki, Professor at the Silesian University of Technology, Department of Welding, Silesian University of Technology in Gliwice

welding conditions. Traditional welding technologies are not always capable of satisfying strict criteria connected with the welding of advanced high strength steels and, as a result, are not able to ensure the required quality and the strength of welded joints. The aforementioned issue was discussed by Holzner A. and Górka J. et al. [5–6]. For this reason, industries worldwide see the continuous search for new and specialist welding technologies, based on, e.g. laser welding or hybrid laser arc welding processes (HLAW) [7]. As can be seen in numerous publications, owing to high laser beam power, laser welding enables the obtainment of high penetration depth-weld width ratios, yet it requires the precise preparation of joints and the accurate positioning of the laser welding head in relation to a workpiece. Because of the significant inertia of robotic systems, the above-presented requirements entail the reduction of welding head travel rates and necessitate pressing the edges of elements being joined (butt welded joint) [7–9].

Hybrid welding (laser + MAG) involves the simultaneous application of two heat sources, i.e. laser beam radiation and electric arc. In comparison with "conventional" laser welding, the hybrid welding process is characterised by significantly higher tolerance as regards the width and the shape of the weld grove, but also by significantly lower welding rates and shallower penetration depth. One of the advantages of the aforesaid hybrid welding method is the possibility of joining sheets of significant thicknesses without the special preparation of edges of elements, which translates into the reduction of welding process-related costs [9].

The research discussed in the article aimed to analyse the effect of basic laser welding process parameters (i.e. laser beam power, welding rate and welding linear energy) applied when joining 4.0 mm thick sheets made of advanced high strength steel S960QL on the quality and properties of simulated butt welded joints made using a TruDisk 3302 Yb:YAG disk laser (Trumpf) (having a maximum power of 3.3 kW and featuring a head focusing the laser beam diameter to 200 μm).

Tests

Research-related tests consisted in the performance of the simulated laser welding of 4.0 mm thick butt welded joints (using the bead-on-plate technique) made of steel S960QL. As a result, at the initial stage of the tests it was possible to eliminate the effect of sheet preparation tolerance, variable gap width or the inaccurate positioning of the sheets. The tests involved the use of sheets (150 mm x 225 mm x 4 mm) made of high strength steel S960QL (Tables 1 and 2). The laser welding process was performed using an automated test rig equipped with a TruDisk 3302 disk laser (TRUMPF) (Fig. 2, Table 3).

The identification of the effect of laser welding process parameters on the shape of the weld bead and the depth of penetration as well as the determination of welding parameters enabling the obtainment of proper test joints at subsequent stages required the performance of initial laser welding tests in relation to various laser beam positions, various welding rates and, consequently, various values of welding linear energy. The primary criterion governing the adjustment of welding

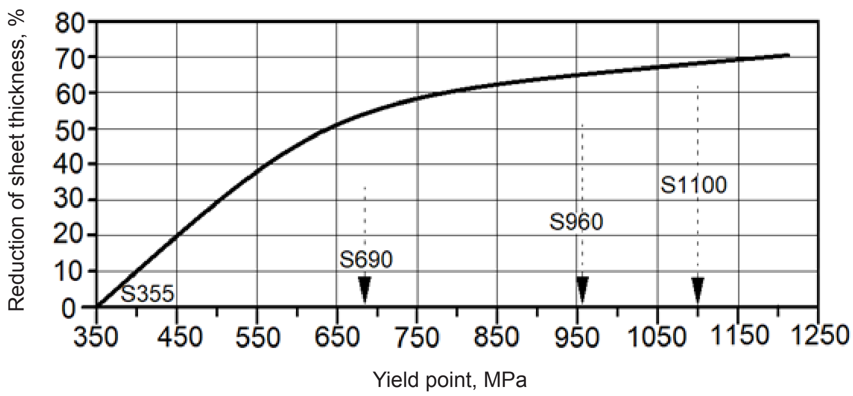

Fig.1. Reduction of required sheet thicknesses in terms of steels characterised by high plastic strength in comparison with steel S355 [4]

Table 1. Chemical composition of high strength steel S960QL in accordance with PN-EN 10025-6 [10]

Chemical composition content, % by weight											
C	**Mn**	**Si**	**V**	**Cr**	**Cu**	**Ni**	**P**	**S**	**Mo**	**Others**	**CEV**
max 0.20	max 1.70	max 0.80	max 0.12	max 1.50	max 0.50	max 2.0	max 0.02	max 0.01	max 0.70	Nb: 0.06 Ti: 0.05 Zr: 0.15 N:0.015 B: 0.005	max 0.82

parameters enabling the obtainment of proper test joints was connected with ensuring the full penetration of sheets across their entire thickness as well as the obtainment of the narrowest possible width of the weld face and that of the weld root (Fig. 3, Table 4). Before the tests, the sheet surfaces were subjected to mechanical cleaning and degreasing with acetone. The first six beads, having an approximate length of 60 mm, were used in macro and microscopic metallographic tests as well as in hardness measurements. In turn, the two additional beads, each having a length of 140 mm, were used in impact strength tests performed at various temperatures (Fig. 3).

The macroscopic metallographic tests were performed using an SZX9 stereoscopic microscope (Olympus), whereas the microscopic observations involved the use of a GX71 light microscope (Olympus) (enabling the electronic recording of images). To reveal their structure, the metallographic specimens were subjected to etching in Ma11Fe (Adler's reagent), composed of hydrochloric acid (35%), iron chloride ($FeCl_3 \times 6H_2O$), ammonium chloride (NH_4Cl) and copper chloride ($CuCl_2$). The specimens were observed using a magnification of up to 1000 times.

The microhardness measurements were performed in accordance with the PN-EN ISO 6507-1 standard, using the Vickers hardness test and a 401 MVD microindentation hardness tester (Wilson Wolpert). The hardness measurements involved the use of the aforesaid metallographic specimens, an indenter load of 0.5 kg and a measurement time of 15 s. Except for specimen no. 2 (characterised by incomplete penetration), microhardness was measured along two lines, with measurement points located every 0.5 mm. In relation to the narrowest beads having the narrow HAZ, measurement points were located every 0.2 mm.

The impact strength tests involved specimens having dimensions of 50 mm × 10 mm × 8 mm and notch V=2 mm (Fig. 4). The tests were performed using a SUNPOC Impact Tester at a temperature of -20°C, 0°C and 20°C. The V-notch was made on the weld face side. The tests were performed in accordance with the PN-EN ISO 9016 standard. The fractures were observed using a scanning electron microscope (SEM). The chemical composition of the micro-areas was analysed and precipitates were identified using energy dispersive spectrometry (EDS).

Table 2. Mechanical properties of high strength steel S960QL in accordance with PN-EN 10025-6 [10]

Parameter	**Value**
Elongation, A_5, %	$A_5 \geq 10$
Yield point R_{eH} , MPa	≥ 960
Tensile strength R_m , MPa	980–1150
Impact energy at 0°C, KV, J	35
Impact energy at -20°C, KV, J	30
Impact energy at -40°C, KV, J	27

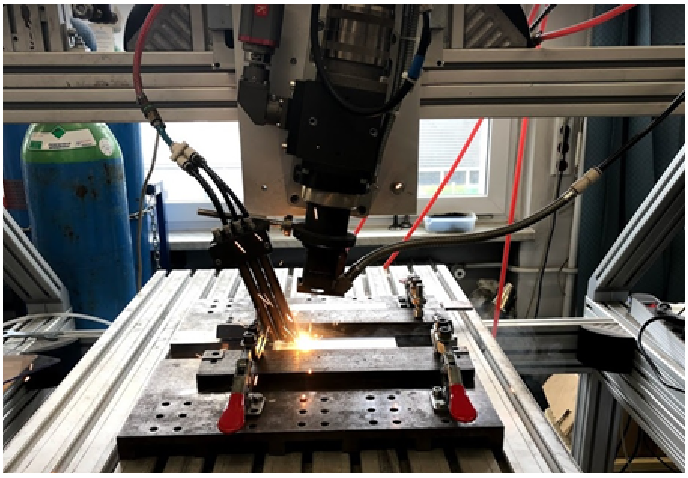

Fig. 2. Automated test rig provided with the TruDisk 3302 disk laser (Trumpf) and the butt laser welding of 4.0 mm thick joints in high strength steel

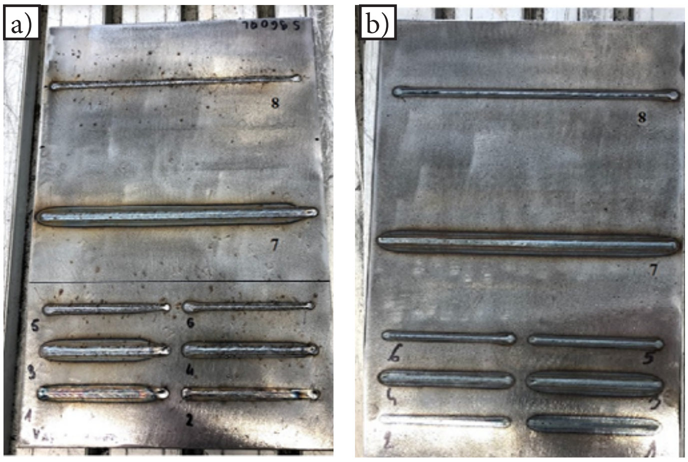

Fig. 3. Face (a) and root (b) of the test beads after laser melting tests (simulated welding of butt joints) involving 4.0 mm thick sheets made of high strength steel S960QL; process parameters as specified in Table 4

Table 3. Specifications of the TruDisk 3302 disk laser (Trumpf)

Parameter	**Value**
Laser radiation wavelength, nm	1030
Maximum laser beam power, W	3300
Laser beam divergence, mm mrad	8.0
Diameter of the core of the optical fibre transmitting the laser beam, μm	200
Optical fibre length, m	20
Lens focal length, mm	200
Collimator focal length, mm	200
Laser beam focus diameter, μm	200

Note: optical fibre type: LLK-D 02/20

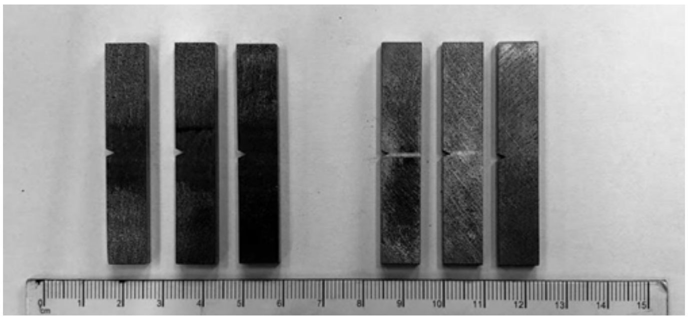

Fig 4. Specimens made of steel S960QL used in the impact strength tests

Table 4. Parameters used in the laser melting (simulated welding of butt joints) of 4.0 mm thick sheet made of high strength steel S960QL

Bead no./ Spec. no.	Location of the laser beam focus in relation to the upper surface of the sheet [mm]	Laser beam power [kW]	Melting rate [m/min]	Melting linear energy [J/mm]	Visual assessment of penetration
1	+5	3.3	1.0	198	FP
2	+5		1.5	132	LP, FU
3	0		1.0	198	FP, FU, MS, C
4	0		1.5	132	FU, FP, MS, C
5	0		2.0	100	NP, FU, MS
6	0		2.5	80	FU, NP, EWMR, MS
7	0	3.3	1.0	198	FP, FU
8	0		2.5	80	NP, FU, EWMR

Remaining parameters: laser beam focus diameter – 200 m, shielding gas – Ar (99.999%), shielding gas flow rate – 15 l/min; bead quality assessment: LP – lack of penetration, FP – full penetration, NP – narrow penetration, FU – face undercut, MS – material spatter, C – crater at the end of the bead, EWMR – excess weld metal on the root side

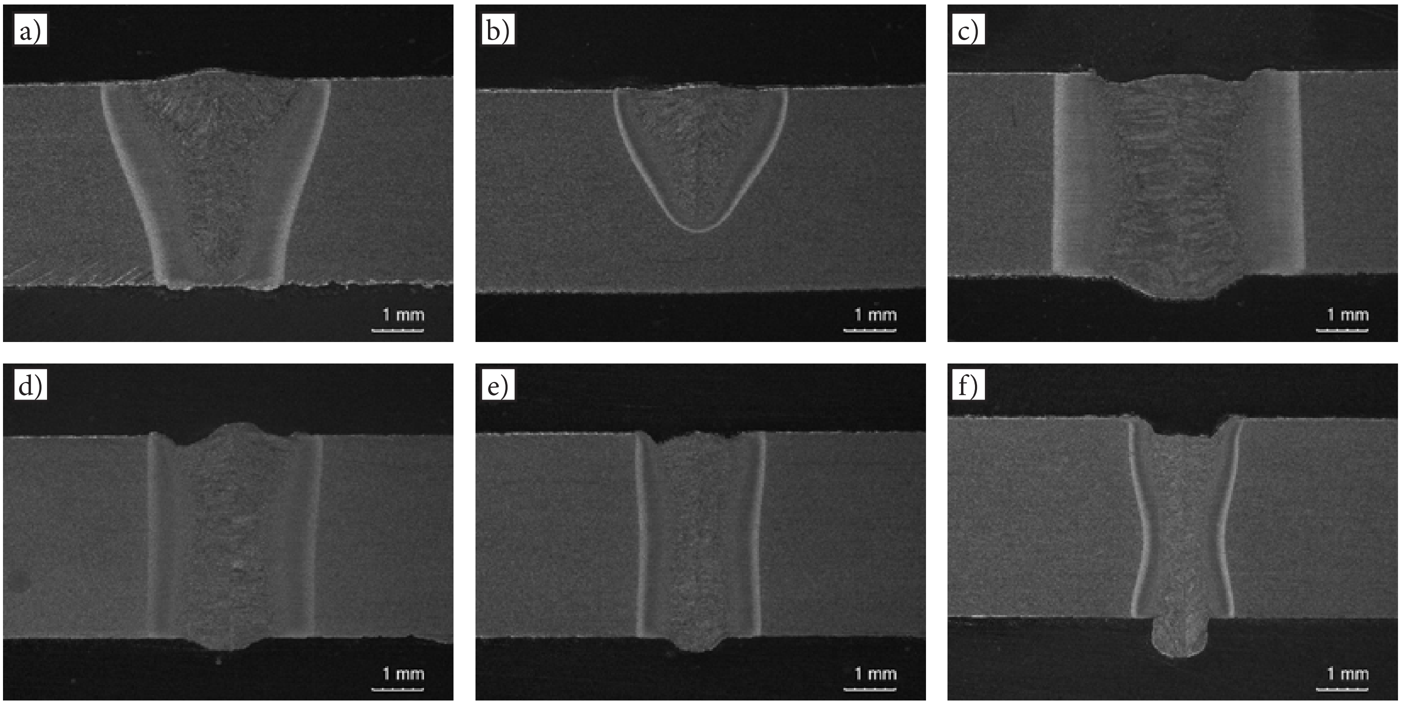

Fig. 5. Macrostructure of the beads made using the method of the simulated laser welding of butt joints in 4.0 mm thick high strength steel S920QL; TruDisk 3302 disk laser (Trumpf); etching: Adler's reagent II; designations as in Table 4: a) bead no. 1, b) bead no. 2, c) bead no. 3, d) bead no. 4, e) bead no. 5 and f) bead no. 6

The microhardness measurements concerning the butt joints of 4.0 mm thick sheets made of high strength steel S960QL and welded using the TruDisk 3302 disk laser were performed in accordance with the PN-EN 6507-1 standard and the schematic diagram presented in Figure 10. Depending on the width of the weld and that of the HAZ, the distance between successive measurement points amounted to 0.5 mm or 0.2 mm.

The impact strength tests concerning the specimens obtained using the technique of the simulated laser welding of butt joints of 4.0 mm thick sheets made of high strength steel S960QL were performed at a temperature of-20°C, 0°C and 20°C, in accordance with the PN-EN ISO 9016 standard. The main view of the specimens after the test is presented in Figure 15, whereas the test results are presented in Table 5.

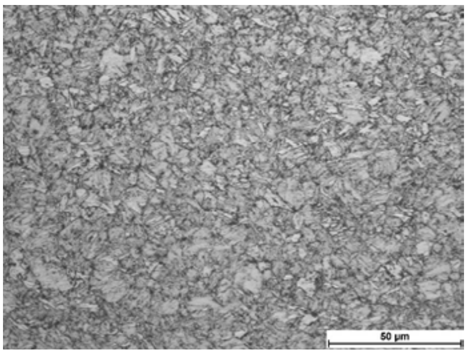

Fig. 6. Microstructure of the base material of the sheets made of high strength steel S960QL in the as-received state; etchant: Adler II

Table 5. Impact strength test results concerning the specimens obtained using the technique of the simulated laser welding of butt joints of 4.0 mm thick sheets made of high strength steel S960QL

Welding rate [m/min]	Temperature [°C]	Impact energy [J]			Average value [J]	Impact strength tests [J/cm²]			Average impact strength value [J/cm²]
1.0	20	28	22	29	26.33	87.5	68.75	90.62	82.29
	0	22	21	24	22.33	68.75	65.62	75	69.79
	-20	22	19	18	19.66	68.75	59.37	56.25	61.46
2.5	20	26	36	19	27	81.25	112.5	59.37	84.37
	0	20	21	12	17.66	62.5	65.62	37.5	55.20
	-20	19	11	13	14.33	59.37	34.37	40.62	44.78

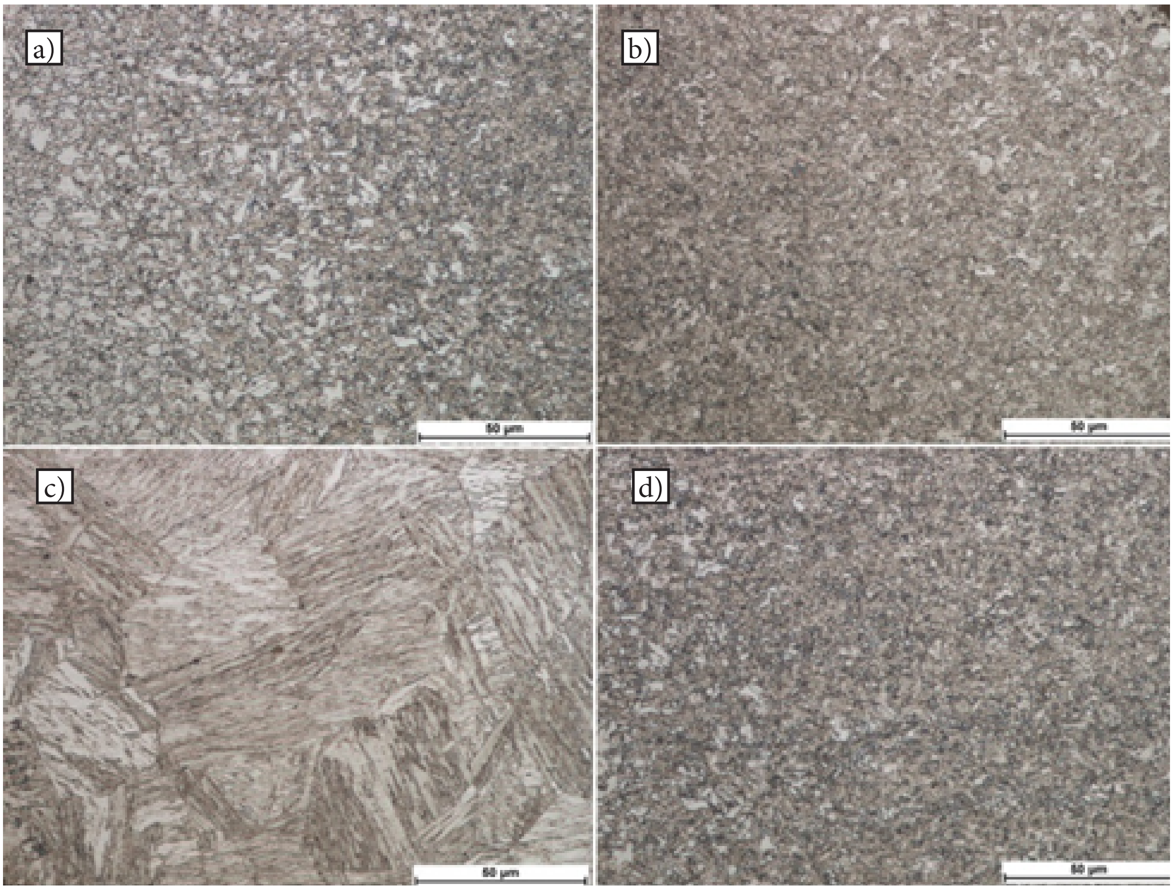

Fig. 7. Microstructure of the simulated butt joint of the 4.0 mm thick sheets made of high strength steel S960QL (specimen no. 1, focus location: +5 mm, laser beam power: 3.3 kW, welding rate: 1.0 m/min, as in Table 4), where A) BM-HAZ interface, B) penetration, C) HAZ and D) area near the fusion line

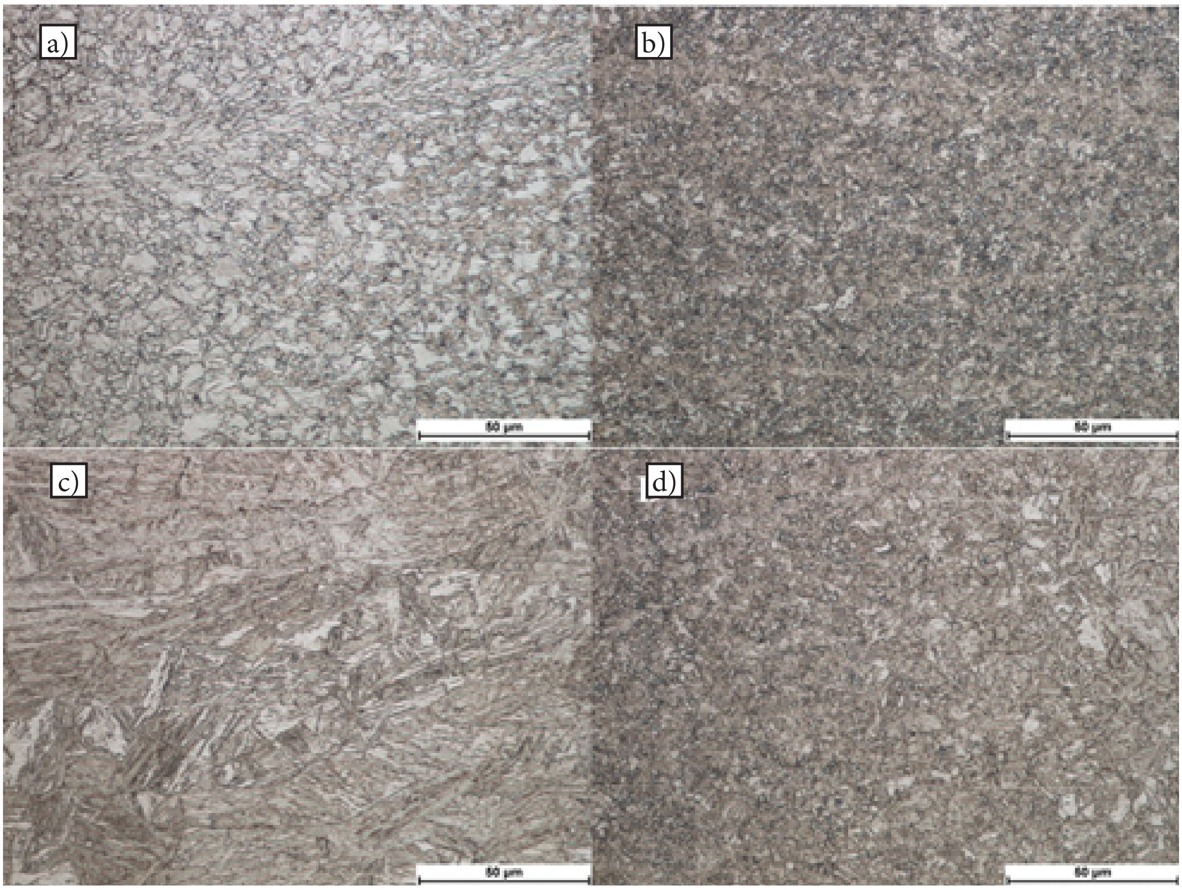

Fig. 8. Microstructure of the simulated butt joint of the 4.0 mm thick sheets made of high strength steel S960QL (specimen no. 3, laser beam focused on the upper surface of the sheet, laser beam power: 3.3 kW, welding rate: 1.0 m/min, as in Table 4), where A) BM-HAZ interface, B) penetration, C) HAZ and D) fusion line

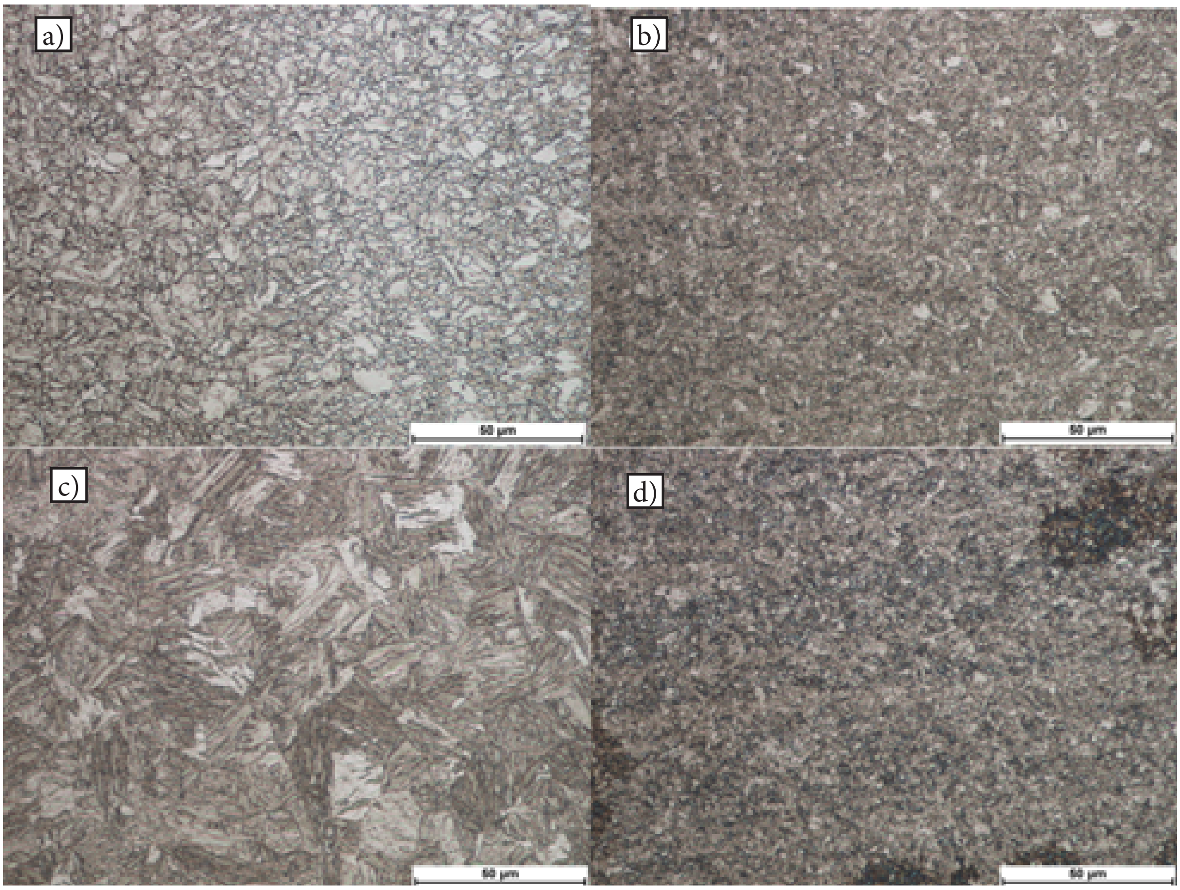

Fig. 9. Microstructure of the simulated butt joint of the 4.0 mm thick sheets made of high strength steel S960QL (specimen no. 4, laser beam focused on the upper surface of the sheet, laser beam power: 3.3 kW, welding rate: 1.5 m/min, as in Table 4), where A) BM-HAZ interface, B) penetration, C) HAZ and D) fusion line

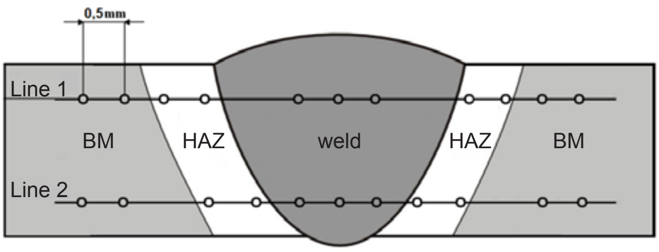

Fig. 10. Schematic diagram presenting microhardness measurements in the cross-section of the specimens

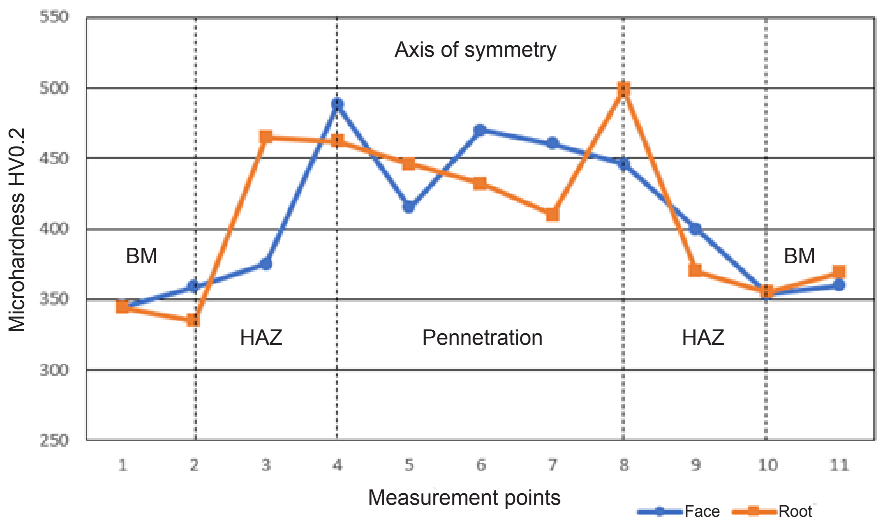

Fig. 11. Distribution of microhardness in the cross-section of the beads obtained using the technique of the simulated laser welding of butt joints of 4.0 mm thick sheets made of high strength steel S960QL and welded using the TruDisk 3302 disk laser; specimen no. 1 in Table 4

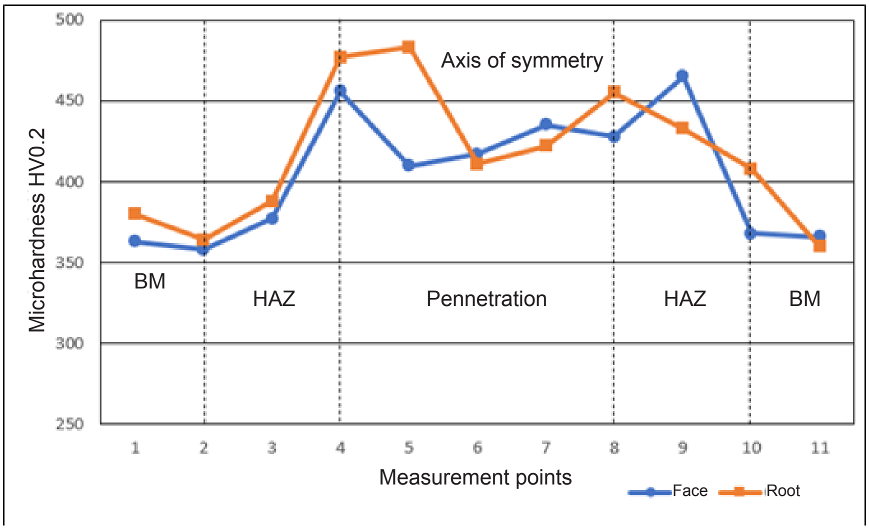

Fig. 12. Distribution of microhardness in the cross-section of the simulated butt joint of 4.0 mm thick sheets made of high strength steel S960QL and welded using the TruDisk 3302 disk laser; specimen no. 3 in Table 4

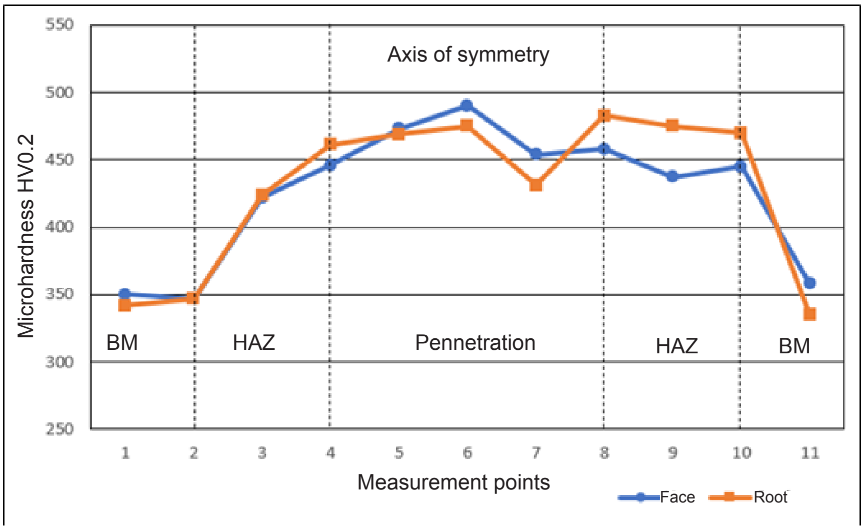

Fig. 13. Distribution of microhardness in the cross-section of the simulated butt joint of 4.0 mm thick sheets made of high strength steel S960QL and welded using the TruDisk 3302 disk laser; specimen no. 4 in Table 4

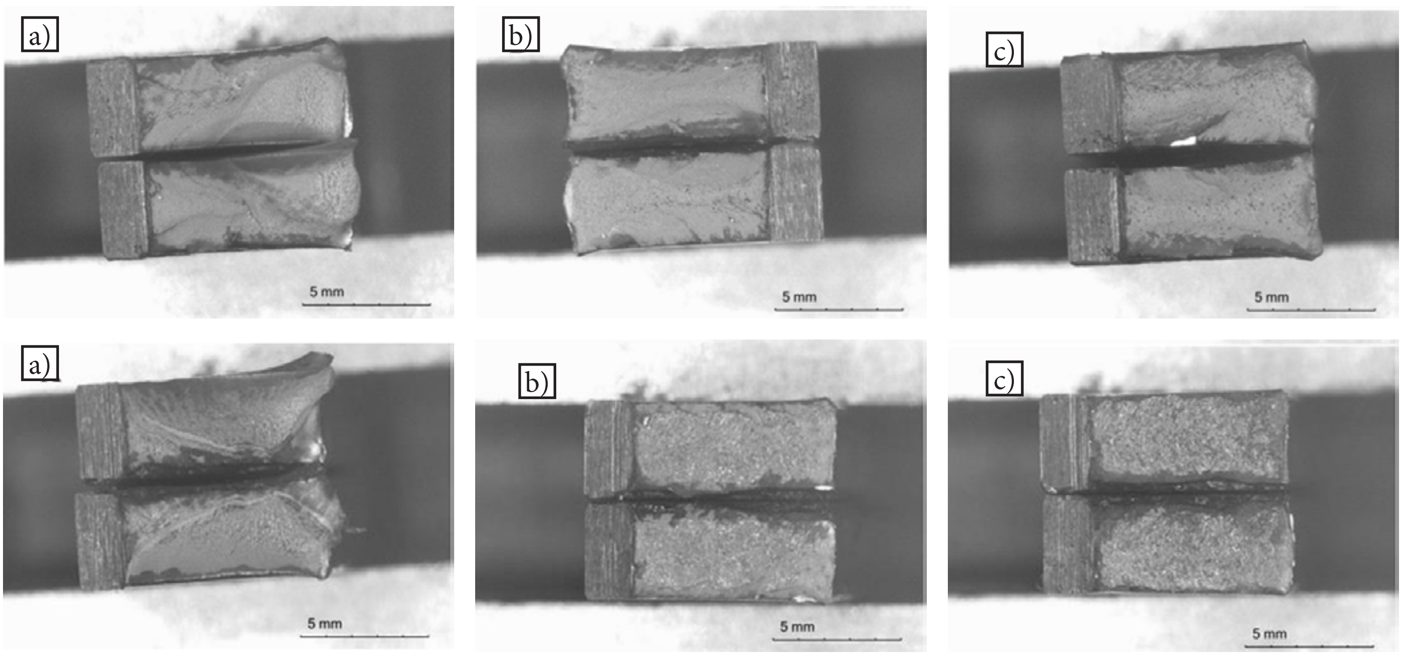

Fig. 14. Impact strength test results concerning the specimens obtained using the technique of the simulated laser welding of butt joints of 4.0 mm thick sheets made of high strength steel S960QL and welded using the TruDisk 3302 disk laser; welding rate v = 1 m/min. (top line) and v = 2.5 m/min (bottom line), where A) 20°C, B) 0°C and C) -20°C

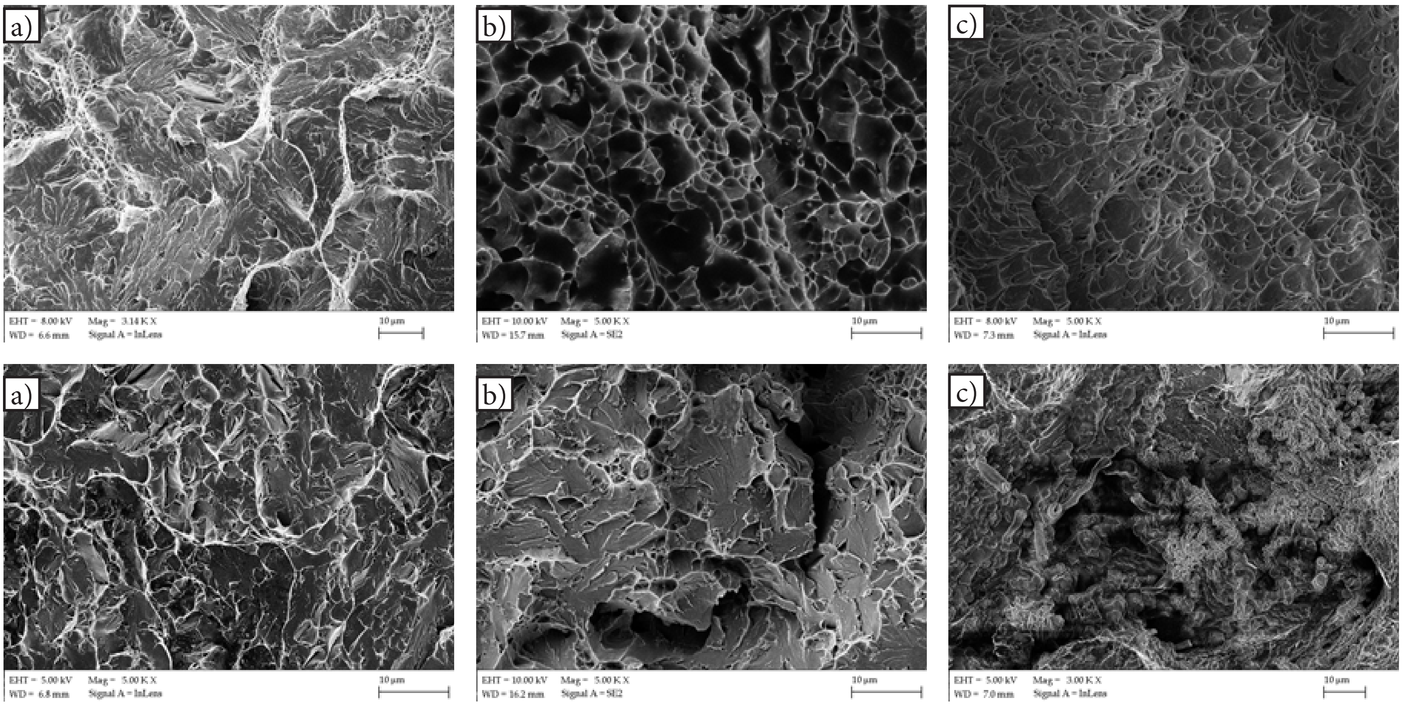

Fig. 15. Fractographic test results concerning the specimens obtained using the technique of the simulated laser welding of butt joints of 4.0 mm thick sheets made of high strength steel S960QL and welded using the TruDisk 3302 disk laser; welding rate v = 1 m/min. (top line) and v = 2.5 m/min (bottom line), where A) 20°C, B) 0°C and C) -20°C

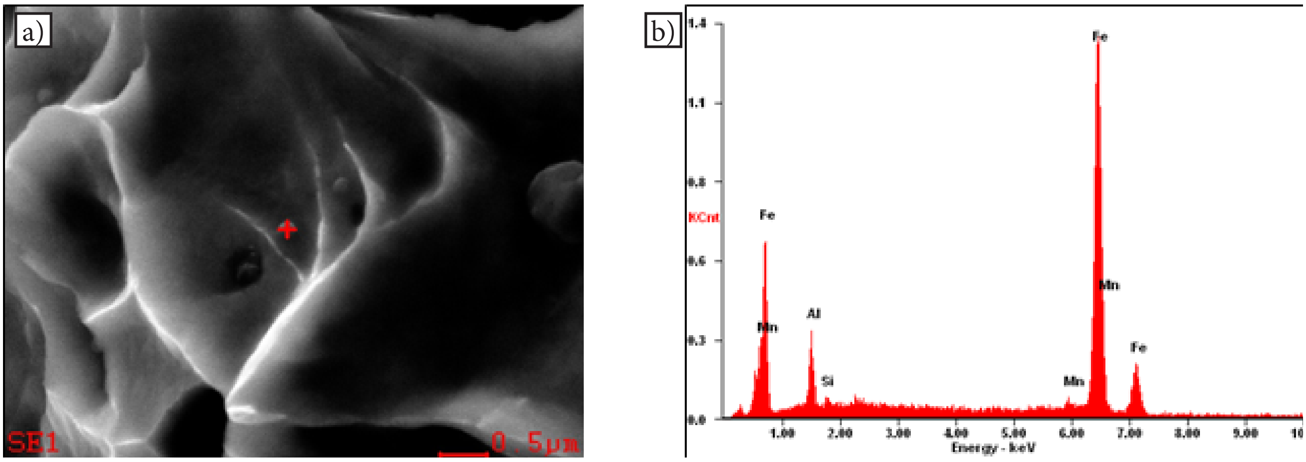

Fig. 16. Fractographic image (SEM) of the specimen made using a welding rate of 1.0 m/min, after the impact strength test performed at a temperature of 0oC (a) and the spectrum (EDS) of the surface of a spherical particle located on the surface of the fracture (b)

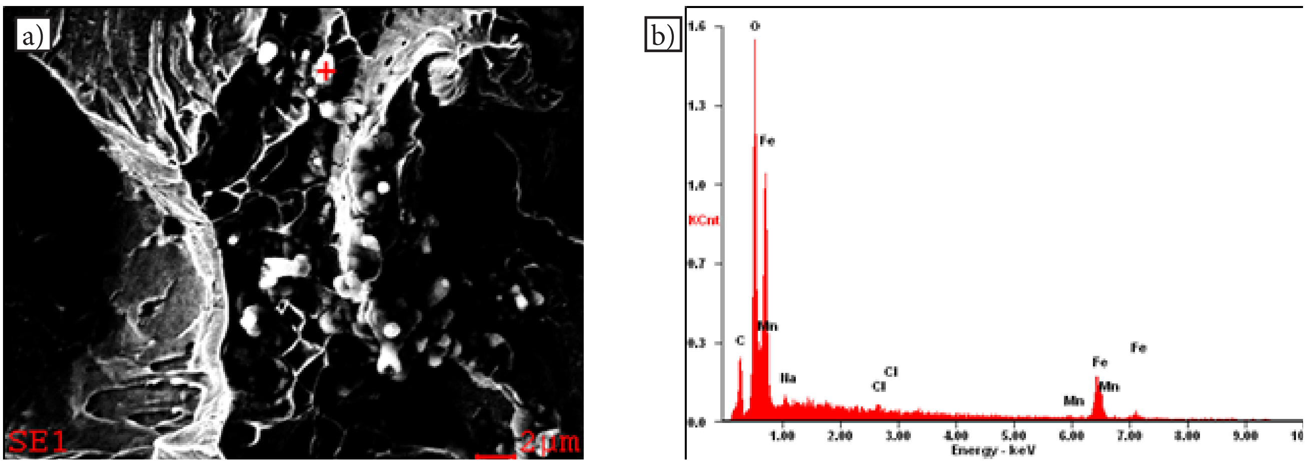

Fug. 17. Fractographic image (SEM) of the specimen made using a welding rate of 2.5 m/min, after the impact strength test performed at a temperature of -20oC (a) and the spectrum (EDS) of the surface of a spherical particle located on the surface of the fracture (b)

Analysis of test results

The visual tests (Fig. 3) revealed that not all of the specimens made using the defined set of laser welding parameters satisfied previously specified quality-related criteria. Because of the lack of penetration in specimen no. 2 as well as significant weld face undercuts in some other specimens, subsequent tests included the specimens made using the laser beam focused on the upper surface (of a given specimen), a linear energy of nearly 200 J/mm and a minimum linear energy of 80 J/mm. Figure 5 presents the effect of the laser welding rate and a constant laser beam power of 3.3 kW on the shape of the fusion line, the width of the weld and the width of the HAZ. An increase in the laser welding rate and a simultaneous decrease in linear energy were accompanied by a decrease in the width of penetration and a decrease in the width of the HAZ. Figure 5f presents the excessive incompletely filled groove and the excess weld metal on the root side.

The tests and microscopic observations revealed that the base material of the sheet made of steel S960QL was characterised by the fine-grained structure of tempered martensite (Fig. 6). In turn, the tests and observations concerned with the microstructure in the cross-section of penetration (of the simulated butt welded joints) revealed that, within the investigated range of parameters and linear energy, the microstructure in the penetration area and that in the HAZ were similar. The structure observed in the HAZ changed along with the distance from the fusion line, where the initial area of the base material side was characterised by clearly visible grain size refinement. The penetration area contained primarily lamellar martensite. In turn, on the metallographic specimen plane it was possible to observe acicular martensite. The formation of the acicular martensite resulted from the cross-cutting of the space structure with the plane (see Figures 7b, 8b and 9b).

The microhardness measurements revealed that the microhardness of the base material of the 4.0 mm thick sheets made of steel S960QL changed within the range of 345 HV0.2 to 470 HV0.2 (Figures 11–13). The highest hardness, observed in the HAZ, amounted to approximately 500 HV0.2 (Figures 11–13). In turn, the microhardness in the penetration area was restricted within the range of approximately 420 HV0.2 to 470 HV0.2. The significant hardness increase in the penetration area and in the HAZ was not favourable as it could result in the reduction of welded joint toughness.

The impact strength tests revealed that the specimens made using the higher welding rate (i.e. 2.5 m/min) and lower welding linear energy were characterised by significantly lower toughness (particularly at lower temperatures) than those made using higher linear energy. For instance, the impact energy of the specimens made with higher linear energy (i.e. 198 J/mm) amounted to 22.3 J at a temperature of 0°C. In turn, the impact energy of the specimens made using lower linear energy (i.e. 80 J/mm) amounted to 17.7 J. Even greater differences were observed in relation to the results of the tests performed at a temperature of -20°C, where the impact energy of the specimen made using higher linear energy amounted to 19.7 J, whereas that of the specimen made using lower linear energy amounted to a mere 14.3 J (see Table 5). The detailed SEM-based microstructural observations as well as the analysis of the structure in the penetration area and in the HAZ revealed that the aforesaid situation was triggered by the presence of lamellar martensite in the specimen fusion area.

Excessively high cooling rates during the laser welding of the 4.0 mm sheets made of steel S960QL were unfavourable as they increased the content of lamellar martensite, thus reducing material ductility. Figure 14 presents the surfaces of the fractographic specimens used in the impact strength tests, revealing clearly visible differences of all the fractures in relation to various values of welding linear energy.

The fractographic impact strength test-related results concerning the specimens obtained using the technique of the simulated laser welding of butt joints of 4.0 mm thick sheets made of high strength steel S960QL and welded using the TruDisk 3302 disk laser (welding rates v = 1 m/min and v = 2.5 m/min) are presented in related microphotographs (Fig. 15). The observations of the fractures at a temperature of 20°C revealed the presence of a transcrystalline ductile fracture (Fig. 15a). The plastically strained area was characterised by numerous convexities and concavities (craters) containing spherical precipitates. The surface of ductile fractures is usually expanded. When observed by the unaided eye, the surface of ductile fractures is grey and characterised by fibrous morphology. The observations were concerned with the ductile fractures of the specimens subjected to impact strength tests performed at a temperature of up to -20°C (Fig. 15c). However, at a temperature of -20°C it was also possible to observe slight traces of cleavable areas and microcracks, particularly visible in the specimens made using the higher welding rate (i.e. 2.5 m/min) and, consequently, lower welding linear energy.

The SEM-based microstructural observations performed at high magnification revealed the presence of spherical particles as well as of nanometrically-sized particles of irregular shapes, located primarily in hollows situated on the fracture surface. The EDS-based test results revealed that the aforesaid particles were primarily oxides arranged dispersively in the weld area (Fig. 16).

It could be stated that, because of the chemical composition of steel S960QL, its high carbon equivalent and susceptibility to martensitic transformation, the lowest laser welding-related linear energy values were favourable as they increased the content of martensite in the penetration area (i.e. in the weld of the simulated joint) and, as a result, were responsible for decreased toughness, particularly at lower temperatures.

Concluding remarks

The above presented test results concerning the simulated laser welding of 4.0 mm thick sheets made of high strength steel S960QL using the disk laser justified the formulation of the following conclusions:

- as regards laser welding without the use of the filler metal, the obtainment of the proper shape of the weld, i.e. with full penetration and without undercuts, required the precise adjustment of welding parameters;
- in terms of the sheets made of steel S960QL, low values of laser welding linear energy were responsible for a significant increase in hardness in the weld and in the HAZ (even up to 500HV0.2);
- increased laser welding rates (within the range of specified technological conditions) and, at the same time, decreased welding linear energy were responsible for the increased content of martensite (in relation to bainite) in the penetration area (weld) and the decreased toughness of the test specimens, particularly at lower temperatures.

References

[1] Li G.J., Liu X.L.: Literature review on research and development of automotive lightweight technology. Mater. Sci. Technol., 2020, no. 28, pp. 47–61.

[2] Ohjoon K., Lee K.Y., Kim G.S., Chin K.G.: New trends in advanced high strength steel developments for automotive application. Mater. Sci. Forum, 2010, no. 884, pp. 136–141.

[3] Goss C., Marecki P., Muszyński T., Torzewski J.: Badania porównawcze połączeń spawanych ze stali wysoko wytrzymałych stosowanych na konstrukcje pojazdów specjalnych. TTS Technika Transportu Szynowego, 2015, vol. 22, no. 12, pp. 572–575.

[4] Urbańczyk M., Adamiec J., Łyczkowska K.: Spawanie hybrydowe laser + MAG stali o podwyższonej granicy plastyczności

S960QL. Spajanie, 2018, no. 4 (42), pp. 14–18.
[5] Holzner A.: Spawanie wysokowytrzymałych drobnoziarnistych stali konstrukcyjnych metodą MAG drutami proszkowymi. Biuletyn Instytutu Spawalnictwa, 2011, no. 4, pp. 39–48.
[6] Górka J., Miler G.: Wpływ kierunku walcowania blach ze stali obrobionej termomechanicznie na jakość złączy spawanych. Przegląd Spawalnictwa, 2010, no. 7, pp. 8–19.
[7] Kurc-Lisiecka A., Lisiecki A.: Weld metal toughness of autogenous laser welded joints of high strength steel Domex 960. Materials Performance and Characterization no. 8 (6), 2019, Special Issue on Laser Processing of Materials, Guest Editor: Leszek A. Dobrzański, DOI: 10.1520/MPC20190071.
[8] Grajcar A.: Technologie łączenia wysokowytrzymałych blach stalowych dla motoryzacji. Stal, Metale & Nowe Technologie, 2016, no. 9–10, pp. 39–43.
[9] Morawiec M., Grajcar A., Różański M., Stano S.: Porównanie mikrostruktury i twardości stali ASHH spawanych laserowo. Sympozjum Katedr i Zakładów Spawalnictwa pt. Nowoczesne zastosowania technologii spawalniczych, Istebna 14–15 June 2016 r., pp. 295–301, ISBN 978-83-63605-50-6.
[10] PN-EN 10025-6:2019: Wyroby walcowane na gorąco ze stali konstrukcyjnych – Część 6: Warunki techniczne dostawy wyrobów płaskich o podwyższonej granicy plastyczności w stanie hartowanym i odpuszczonym.